# ERO1-independent production of $H_2O_2$ within the endoplasmic reticulum fuels Prdx4 mediated oxidative protein folding

Running title: "An ER source for $H_2O_2$"

Tasuku Konno[1], Eduardo Pinho Melo[2], Carlos Lopes[2], Ilir Mehmeti[4], Sigurd Lenzen[4], David Ron[1,*], Edward Avezov[1,*]

[1]University of Cambridge, Cambridge Institute for Medical Research, the Wellcome Trust MRC Institute of Metabolic Science and NIHR Cambridge Biomedical Research Centre, Cambridge, CB2 0XY, United Kingdom

[2]Center for Biomedical Research, Universidade do Algarve, Faro, Portugal

[4]Institute of Clinical Biochemistry, University of Hannover Medical School

[*]Corresponding authors:

Edward Avezov ea347@cam.ac.uk or David Ron dr360@medschl.cam.ac.uk
Cambridge Institute for Medical Research,
University of Cambridge, Wellcome Trust/MRC Building
Cambridge Biomedical Campus, Hills Road
Cambridge CB2 0XY
United Kingdom
Phone 01223 768 940

(19839 characters)

## Abstract:

The endoplasmic reticulum (ER) localized peroxiredoxin 4 (PRDX4) supports disulfide bond formation in eukaryotic cells lacking the ER oxidase ERO1. The source of peroxide that fuels PRDX4-mediated disulfide bond formation has remained a mystery, as ERO1 is believed to be a major producer of $H_2O_2$ in the ER lumen. We report on a simple kinetic technique to track $H_2O_2$ equilibration between cellular compartments suggesting that the ER is relatively isolated from cytosolic or mitochondrial $H_2O_2$ pools. Furthermore, expression of an ER-adapted catalase to degrade lumenal $H_2O_2$ attenuated PRDX4-mediated disulfide bond formation in cells lacking ERO1, whilst depletion of $H_2O_2$ in the cytosol or mitochondria had no similar effect. ER catalase did not effect the slow residual disulfide bond formation in cell lacking both ERO1 and PRDX4. These observations point to exploitation of a hitherto unrecognized lumenal source of $H_2O_2$ by PRDX4 and a parallel slow $H_2O_2$-independent pathway for disulfide formation.

(150 words)

## eTOC:

Molecular oxygen and peroxides both contribute to oxidative folding of secreted proteins in eukaryotes. Tracking the kinetics of equilibration of $H_2O_2$ between compartments revealed unexpected isolation of the endoplasmic reticulum and hints at a hitherto unsuspected local source of peroxide.

(40 words)

## Introduction:

Oxidative protein folding in the ER relies on a Protein Disulfide Isomerase (PDI) machinery that accept electrons from client cysteine thiols generating native disulfides (Hudson et al., 2014). A major advance in our understanding of this machinery came with discovery of an ER-localized PDI oxidase, ERO1 (Frand and Kaiser, 1998; Pollard et al., 1998), that accepts electrons from reduced PDI and hands them over to molecular oxygen, catalyzing oxygen-mediated disulfide bond formation (Araki et al., 2013; Tsai and Rapoport, 2002). ERO1 is conserved in eukaryotes. The marked impairment in disulfide bond formation in yeast lacking ERO1 suggested an essential role in accelerating dithiol oxidation in the ER (Frand and Kaiser, 1998; Pollard et al., 1998). Surprisingly, targeted mutagenesis of the genes encoding animal ERO1 orthologues, *ERO1L*/ERO1$\alpha$ and *ERO1LB*/ERO1$\beta$ revealed a remarkably mild phenotype (Tien et al., 2008; Zito et al., 2010a).

In ERO1 deficient cells and tissues, life-sustaining rates of disulfide bond formation depend on the ER-localized enzyme Peroxiredoxin 4 (PRDX4) (Zito et al., 2012; Zito et al., 2010b). PRDX4 accepts electrons from reduced PDI and transfers them to hydrogen peroxide (Tavender et al., 2010; Zito et al., 2010b). ERO1-mediated electron transfer from reduced PDI to oxygen, reduces the latter to $H_2O_2$ (Gross et al., 2006). Thus, the sequential action of ERO1 and PRDX4 can produce two disulfides from every molecule of oxygen converted to water.

Dispensable, under normal circumstances (Iuchi et al., 2009), the PRDX4-mediated reaction becomes limiting in cells lacking ERO1 (Zito et al., 2010b), but the identity of the source of $H_2O_2$ that fuels PRDX4 in cells lacking ERO1 is unknown. Resolving this mystery has been hampered by difficulties in measuring changes in $H_2O_2$

concentration in the ER of living cells. To circumvent this issue we have exploit the kinetic properties of intra-vital fluorescent thiol redox probes that diverge in their reactivity with the oxidized/reduced PDI couple and $H_2O_2$. Our studies point to an ER-localised, ERO1-independent source of $H_2O_2$ that fuels PRDX4-mediated disulfide bond formation in cells lacking ERO1.

## Results and discussion:

### PRDX4-mediated ER thiol oxidation is fueled by hydrogen peroxide independently of ERO1

Combined deficiency of ERO1 and PRDX4 is detrimental to mammalian development and enhances lethality of mutant mice. Nonetheless, enfeebled, viable compound mutant cell lines can be cultured in vitro (Zito et al., 2012). Remarkably, such triple mutant cells *Ero1l*$^{Gt(xst171)Byg/Gt(XST171)Byg}$; *Ero1lb*$^{Gt(P077G11)Wrst/Gt(P077G11)Wrs}$; *Prdx4*$^{tm1.1JuFu/tm1.1JuFu}$ (abbreviated TKO) defend a steady state PDI thiol redox couple that is indistinguishable from wildtype cells. However the deficit in oxidative power of the TKO cells is revealed in a kinetic assay that tracks recovery of disulfide bonds following a reductive pulse of dithiothreitol (DTT) (Avezov et al., 2013).

Previously these measurements were performed by tracking changes in fluorescent lifetime of ERroGFPiE, an ER-localized intravital fluorescent redox probe that equilibrates rapidly with PDI and is specially tuned to PDI's oxidative state found in the ER (Avezov et al., 2013; Lohman and Remington, 2008). However this theoretical advantage of ERroGFPiE is obviated by the normal steady state of the PDI redox couple in TKO cells. Furthermore the fluorescent lifetime imaging measurements necessary to track the redox state of the ER-tuned roGFPiE, are difficult to acquire. Therefore, we sought an alternative method to detect the kinetic defect in ER thiol re-oxidation observed in the TKO cells following a DTT pulse.

ER-localized roGFP2 (ERroGFP2) is recognized as a substrate by PDI and kinetic parameters deduced from the recovery of its oxidized state following a DTT pulse and washout thus reflect the activity of the enzymatic machinery for PDI re-oxidation in vivo (Tsunoda et al., 2014). Its enhanced brightness enables measuring its redox state ratiometrically, by comparing the emission intensity of the probe at 530 nm when excited

at 405 nm and 488 nm (Hanson et al., 2004), and does not require the more exacting measurements of fluorescent lifetime.

The genetic defect in mouse fibroblasts lacking key ER redox enzymes was confirmed: ERO1α, normally present in fibroblasts, was undetectable in homozygous double knockout mutant *Ero1l*$^{Gt(xst171)Byg/Gt(XST171)Byg}$, *Ero1lb*$^{Gt(P077G11)Wrst/Gt(P077G11)Wrst}$ (DKO) MEFs and in triple knockout mutant (TKO) that are also homozygous for a null allele of *Prdx4*$^{tm1.1JuFu/tm1.1JuFu}$. PRDX4 was readily detected in fibroblasts and was eliminated by mutation of its encoding gene, whereas the pancreatic specific isoform of ERO1, ERO1β, was undetectable in fibroblasts of all genotypes tested (Fig. 1A).

As expected, ERroGFP2 was localized to the ER of transfected mouse fibroblasts (Fig.1B) and was rapidly re-oxidized following a DTT reductive pulse and washout of the reductant (Fig.1C). The conversion of the reduced probe to its oxidized, pretreatment steady state (re-oxidation phase) occurs with a half time ($t_{1/2}$) of 1.7 ± 0.3 min in wildtype MEFs (Fig.1C & 1H), whereas in TKO cells the re-oxidation was ~5 fold slower ($t_{1/2}$ 9.28 ± 0.8 min) (Fig.1D & 1H). These values, obtained for ERroGFP2, are in agreement with earlier measurements performed with the ER tuned probes ERroGFPiL in HT1080 cells and ERroGFPiE in wildtype and TKO MEF cells (Avezov et al., 2013; van Lith et al., 2011).

In cells with wildtype ERO1 activity, PRDX4 has no measureable effect on the rate of ER thiol re-oxidation following a DTT pulse (Fig. S1). Whilst PRDX4 inactivation by excess ERO1-driven $H_2O_2$ production in DTT pulsed cells may underestimate PRDX4's normal role in thiol oxidation (Tavender and Bulleid, 2010), our observations are consistent with the inconspicuous phenotype of *Prdx4*$^{tm1.1JuFu/tm1.1JuFu}$ (PKO) mice (Iuchi et al., 2009). Conversely, lack of ERO1 measurably delayed oxidation kinetics, as a consistently longer $t_{1/2}$ was measured in ERO1 deficient DKO cells (which contain PRDX4,

Fig 1A, lane 2) than in their isogenic control (Fig. 1E & 1H). Nevertheless, the importance of PRDX4 to the kinetics of disulfide bond formation in cells lacking ERO1 was highlighted by the restoration of the $t_{1/2}$ of recovery of oxidized ERroGFP2 in TKO cells transduced with wildtype PRDX4 and by the inactivity of the enzymatically inactive PRDX4$^{C127S}$ mutant lacking the peroxidiac cysteine (Fig. 1F-1H). These observation confirm that PRDX4 assumes an important role in the kinetics of disulfide bond formation when ERO1 activity is limiting, and correlate with the previous phenotypic analysis of compound mutant cells (Zito et al., 2010b).

## Compartment-specific responsiveness of the $H_2O_2$-sensitive probe HyPer reveals a barrier to oxidant diffusion across the ER membrane

The above observations raised the question of the source of the oxidative process that fuels PRDX4 recycling from its reduced to its oxidized state in the ERO1 deficient cells lacking the major known source of $H_2O_2$ production in the ER lumen. To address this question we sought tools to estimate changes in lumenal $H_2O_2$ concentration.

HyPer is a genetically encoded in vivo sensor for fluctuations in $H_2O_2$ concentration. It is based on direct $H_2O_2$–mediated formation of a disulfide bond between peroxidiac cysteine$^{199}$ that reacts with $H_2O_2$ to form a sulfenic acid (and water) and the resolving cysteine$^{208}$ of the *E. coli* peroxide sensor OxyR (Zheng et al., 1998) The intramolecular $C^{199}$-$C^{208}$ disulfide is coupled to changes in the probes' fluorescent properties by incorporating the OxyR sensor into a circularly-permuted YFP (Belousov et al., 2006; Markvicheva et al., 2011). In normally reduced cellular compartments, such as the cytosol and mitochondrial matrix, reduced thioredoxin maintains the OxyR cysteines in their reduced state, ready to respond to $H_2O_2$ (Belousov et al., 2006). In the ER however, HyPer is severely compromised in its ability to sense $H_2O_2$, likely by a competing $H_2O_2$-

independent, disulfide-exchange-mediated formation of a $C^{199}$-$C^{208}$ disulfide (Malinouski et al., 2011; Mehmeti et al., 2012).

Inactivation of ER localized HyPer fits well with our observation that HyPer readily served as a substrate for oxidized PDI (Fig. 2A, S2). However, these same *in vitro* experiments revealed an important kinetic advantage to $H_2O_2$ over oxidized PDI in converting HyPer from its reduced to its oxidized form (Fig. 2A, S2 A & B). To determine if this kinetic advantage could be exploited to sense $H_2O_2$ in the ER, we compared the effect of exogenous $H_2O_2$ on the rate of re-oxidation of ERHyPer with that of ERroGFP2, which is indifferent to $H_2O_2$ (Gutscher et al., 2009), in a DTT washout experiment in TKO cells. $H_2O_2$ enhanced the typically sluggish reoxidation of ERHyPer, but had no effect on ERroGFP2 (Fig. S2 C & D).

The reactivity of HyPer with PDI observed in vitro (Fig. 2A) explains the inactivity of the probe in the ER under baseline conditions (Fig. 2B). Furthermore, in wildtype cells, with a normal complement of ERO1, PDI driven re-oxidation of HyPer dominates, precluding detection of $H_2O_2$. However, if $H_2O_2$ oxidation of HyPer were to exceed the rate of its reduction by a counteracting reductant (e.g. DTT), changes in $H_2O_2$ could be detected in the face of continued presence of a reductant, neutralizing the contribution of PDI. Therefore, we tested the ability of HyPer to respond to $H_2O_2$ in vitro in the presence of DTT.

Figure 2C indicates that in vitro HyPer retains sensitivity to low concentrations of $H_2O_2$ (0-7 μM) in the presence of higher concentration of DTT (2 mM). These features are also observed in vivo, as in wildtype cells exposed continuously to 2 mM DTT (a concentration sufficient to fully reduce PDI thiols), addition of $H_2O_2$ led to a rapid oxidation of ERHyPer but not ERroGFP2 (Fig. 2D & 2E). Re-oxidation of HyPer by $H_2O_2$ in the presence of DTT was faster than that afforded by the core machinery following DTT washout (Fig. 2F,

compare the first and second oxidation phases). Moreover, the presence of DTT had no observable effect on the response of cytosolically-located HyPer (cytoHyPer) exposed to a gradient of $H_2O_2$ (Fig. 3A). These observations are consistent with rapid formation of the OxyR disulfide by reaction with $H_2O_2$ and its slow reduction by DTT, paralleling the hierarchy observed with PDI (Fig. 2A-B).

Having developed a measurement method responsive to exogenously-imposed changes in $H_2O_2$ concentration in the ER, we next set out to compare the responsiveness of cytosolic, mitochondrial and ERHyPer to mounting concentrations of exogenous $H_2O_2$. Remarkably re-oxidation of ERHyPer by exogenous $H_2O_2$ was considerably less efficient than that of the cytosolic or mitochondrially-localised probe (midpoint of 33.2, 13.2 and 12.8 μM of extracellular $H_2O_2$ respectively, Fig. 3B & 3C). To minimize the potential impact of ROS quenching enzymes in the various cellular compartments, we chose to perform these experiments in catalase/peroxidase deficient RINm5F pancreatic cells (Tiedge et al., 1997). In our system this deficiency is manifested by higher sensitivity of cytoHyPer to a gradient of $H_2O_2$ (Fig. 3D).

## The $H_2O_2$ mediated ER-thiol oxidation pathway relies on an internal ER source of the oxidant.

The aforementioned observations suggest the existence of a functional barrier to the rapid diffusion of $H_2O_2$ to the ER and therefore an ER source of $H_2O_2$ to fuel PRDX4-mediated disulfide bond formation, even in cells lacking ERO1. To further explore this possibility, we sought to selectively eliminate $H_2O_2$ from the different compartments by localized expression of catalase and then monitor the effects on ER thiol oxidation rate in DKO cells; a system where this parameter is dependent on $H_2O_2$ fueled PRDX4 activity.

Targeting catalase to the cytosol, mitochondria or ER markedly elevated the total catalase activity in lysates of transfected cells, indicating that the enzyme was active in all

three compartments (Fig. 4A). Activity of catalase was further confirmed by the observation that its presence in any of the three compartments attenuated the response of a co-localised HyPer to exogenous $H_2O_2$ (Fig. 4B-4D). The (obligatory) presence of DTT in the assay of ER catalase (Fig. 4D) and differences in compartment size, obscure the correlation between catalase expression level and the magnitude of the attenuating effect on co-localised HyPer. Nonetheless, our observations point to the activity of catalase in all three compartment.

Despite their ability to degrade cytosolic and mitochondrially-localized $H_2O_2$, neither cytosolic nor mitochondrially localized catalase affected the rate of re-formation of disulfide bonds in the ER: the $t_{1/2}$ to recovery of ERroGFP2 in DKO cells following a DTT pulse was similar in untransfected cells and cells transfected with cytosolic or mitochondrially-localized catalase (Fig. 4E & 4F). By contrast, ER localized catalase markedly attenuated the re-oxidation of the $H_2O_2$ inert ERroGFP2 in DKO cells, increasing its $t_{1/2}$ to recovery from 2.8 ± 0.6 to 10.9 ± 1.24 min (compare the red and purple traces in Fig. 4E). Thus ER catalase eliminates the effect of PRDX4, converting DKO cells to functionally TKO cells.

By contrast, ER catalase had no effect on the rate of ERroGFP2 re-oxidation in TKO cells, lacking the $H_2O_2$-utilising enzyme PRDX4 (Fig 4G). Together, these observations support the conclusion that the attenuated re-oxidation of ERroGFP2 in the DKO cells reflects the depletion of $H_2O_2$, an essential substrate of PRDX4. Moreover, the lack of an effect of ER-catalase on rate of disulfide bond formation in cells lacking PRDX4 (TKO cells, Fig 4G) suggests a non-redundant role for PRDX4 in using ER $H_2O_2$ as an oxidant to drive ER-thiol oxidation in the absence of ERO1 and reports on the existence of additional, slow, residual $H_2O_2$-independent mechanism for disulfide formation in TKO cells.

Our findings are consistent with the evolution of an ER localized ERO1-independent mechanism for disulfide bond formation consisting of PRDX4 and an alternative lumenal source(s) of $H_2O_2$. For now, the physiological significance of this backup mechanism remains obscure, as the bland phenotype of the PRDX4-deficent mouse provides no clues. Nonetheless the finding that the ER membrane poses a barrier to mobility of $H_2O_2$ is consistent with the need to protect the cytosol and nucleus from lumenally-generated $H_2O_2$, which has at least two sources: ERO1 and yet-to-be identified parallel process(es) uncovered here. The cost of sluggish transport across the ER membrane is reflected in a diminished contribution of mitochondrially-generated $H_2O_2$ to ER disulfide bond formation. This fits previous observations whereby inhibition of mitochondrial respiration in ERO1-deficient yeast cells did not affect the ability of PRDX4 to rescue disulfide bond formation (Zito et al., 2010b).

## Materials and Methods:

### Plasmid construction:

Table S1 lists the plasmids used, their lab names, description, published reference and a notation of their appearance in the figures.

### Protein purification and *in vitro* enzymatic assays

Human PDI (PDIA1 18–508) and HyPer were expressed in the E. *coli* BL21 (DE3) strain and purified with Ni-NTA affinity chromatography as previously described (Avezov et al., 2015). Time-dependent changes in redox of HyPer, in the presence of PDI1 or $H_2O_2$, were measured as described (Avezov et al., 2013; Tsunoda et al., 2014). In brief, the ratio of fluorescence emission at 535 nm of samples sequentially excited at 405 nm and 488 nm was measured using Tecan 500 microplate reader (Tecan Group, Mannedorf, CH). For measurements of catalase activity in vitro cells were homogenized in PBS by sonication; decomposition of substrate ($H_2O_2$) was traced by ultraviolet spectroscopy monitoring the absorbance at 240 nm, as described in (Tiedge et al., 1998). Specific activity was calculated using the equation: U/mg = $\Delta$A x $min^{-1}$ x 1000 x ml Reaction Mix / 43.6 x mg Protein, where U is activity units in $\mu$mole $min^{-1}$.

### Transfections, immunoblotting, immunofluorescence and cell culture

Mouse fibroblasts deficient in both ERO1a and ERO1b (DKO cells, genotype: *Ero1l*$^{Gt(xst171)Byg/Gt(XST171)Byg}$; *Ero1lb*$^{Gt(P077G11)Wrst/Gt(P077G11)Wrs}$) (Zito et al., 2010a), and ERO1a and ERO1b deficient cells compounded further by deletion of PRDX4 (TKO cells, genotype: *Ero1l*$^{Gt(xst171)Byg/Gt(XST171)Byg}$; *Ero1lb*$^{Gt(P077G11)Wrst/Gt(P077G11)Wrs}$; *Prdx4*$^{tm1.1JuFu/tm1.1JuFu}$) (Zito et al., 2012) as well as single deficiency of PRDX4 (PKO, genotype *Prdx4*$^{tm1.1JuFu/tm1.1JuFu}$ (Iuchi et al., 2009) and wildtype counterpart cells were cultured in DMEM; RINm5F cells (ATCC, Manassas, VA, USA) were cultured in RPMI (Sigma,

Gillingham, Dorset, UK), both supplemented with 10% fetal calf serum.

Transfections were performed using the Neon Transfection System (Invitrogen, Paisley, UK) applying 3 µg of ERroGFP2 or ERHyPer DNA, 6 µg of PRDX4, 10 µg of catalase DNA/1 x $10^6$ cells.

For immunoblotting cells from confluent 100-mm dishes were washed in phosphate-buffered saline (PBS), lysed in 0.5% Triton X-100, 150 mM NaCl, 20 mM Hepes, pH 7.4, and protease inhibitors. Proteins were resolved by 12% SDS-PAGE and blotted with rabbit ERO1α, ERO1b or PRDX4 antisera (Zito et al., 2010b) or with mouse monoclonal anti-Actin IgG (Abcam, Cambridge, UK)

Prior to immunofluorescence staining cells were fixed with 4% paraformaldehyde, permeabilized with 0.5% Triton X-100/PBS and blocked with 10% goat serum/PBS. To visualize the ER rabbit anti-calreticulin IgG (Pierce, Waltham, MA USA) was used as primary and goat anti-rabbit IgG conjugated to DyLight 543 (Jackson ImmunoResearch Laboratories, West Grove, PA, USA) as secondary antibodies. Catalase was detected using goat IgG (Abcam, Cambridge, UK) as primery and donkey anti goat IgG conjugated to Alexa Fluor488 (Jackson ImmunoResearch Laboratories, West Grove, PA, USA). ERroGFP2 and ERHyPer were detected by their fluorescence. Nuclei were counterstained with Hoechst 33342 (2µg/mL in PBS).

## Confocal microscopy and image analysis

Cells transfected with the redox reporters (roGFP2 or HyPer) were acquired and analyzed by laser scanning confocal microscopy system running Zen Blue software (LSM 510 Meta; Carl Zeiss, Jena, Germany) with a Plan-Apo-chromat 60x oil immersion lens (NA 1.4), coupled to a microscope incubator, maintaining standard tissue culture conditions (37°C, 5% $CO_2$, Okolab), in complete DMEM culture medium. Fluorescence

ratiometric intensity images (512 x 512 points, 16 bit) of live cells were acquired. A diode 405 nm and Argon 488 nm lasers (2 and 0.5% output respectively) were used for excitation of the ratiometric probes in the multitrack mode with an HFT 488/405 beam splitter, the signal was detected with 518-550 nm filters, the detector gain was arbitrary adjusted to yield an intensity ratio of the two channels approximating one.

The recovery half-time was extracted from fitting the intensity ratio changes over time to an exponential equation $I(t) = A(1-e^{-\tau t})$, where I is intensity, t is time, $\tau$ is the fitted parameter. After obtaining $\tau$ from the fitting curve, the recovery half-time was calculated using the formula $t_{1/2} = \ln(0.5)/-\tau$. Images were analyzed using ImageJ (National Institutes of Health, Bethesda, MD, USA) and Zen (Zeiss, Jena, Germany) software.

## Acknowledgments

We are grateful to Joseph E. Chambers (University of Cambridge) for critical comments on the manuscript, James Remington (University of Oregon) for the gift of roGFP plasmids Colin Thorpe (University of Delaware) for the gift of PDI1A plasmids and Rachel Edgar and Akhilesh Reddy (University of Cambridge) for the gift of PRDX4 knockout cells.

Supported by grants from the Wellcome Trust (Wellcome 084812) the European Commission (EU FP7 Beta-Bat No: 277713) and Fundação para a Ciência e Tecnologia, Portugal (PTDC/QUI-BIQ/119677/2010) and, a Wellcome Trust Strategic Award for core facilities to the Cambridge Institute for Medical Research (Wellcome 100140). DR is a Wellcome Trust Principal Research Fellow.

TK was supported by Strategic Young Researcher Overseas Visits Program for Accelerating Brain Circulation, Japan Society for the Promotion of Science (JSPS).

The authors declare no competing financial interests.

## References:


Araki, K., S. Iemura, Y. Kamiya, D. Ron, K. Kato, T. Natsume, and K. Nagata. 2013. Ero1-alpha and PDIs constitute a hierarchical electron transfer network of endoplasmic reticulum oxidoreductases. *The Journal of cell biology*. 202:861-874.

Avezov, E., B.C. Cross, G.S. Kaminski Schierle, M. Winters, H.P. Harding, E.P. Melo, C.F. Kaminski, and D. Ron. 2013. Lifetime imaging of a fluorescent protein sensor reveals surprising stability of ER thiol redox. *The Journal of cell biology*. 201:337-349.

Avezov, E., T. Konno, A. Zyryanova, W. Chen, R. Laine, A. Crespillo-Casado, E.P. Melo, R. Ushioda, K. Nagata, C.F. Kaminski, H.P. Harding, and D. Ron. 2015. Retarded PDI diffusion and a reductive shift in poise of the calcium depleted endoplasmic reticulum. *BMC biology*. 13:2.

Belousov, V.V., A.F. Fradkov, K.A. Lukyanov, D.B. Staroverov, K.S. Shakhbazov, A.V. Terskikh, and S. Lukyanov. 2006. Genetically encoded fluorescent indicator for intracellular hydrogen peroxide. *Nature methods*. 3:281-286.

Frand, A.R., and C.A. Kaiser. 1998. The ERO1 gene of yeast is required for oxidation of protein dithiols in the endoplasmic reticulum. *Molecular cell*. 1:161-170.

Gross, E., C.S. Sevier, N. Heldman, E. Vitu, M. Bentzur, C.A. Kaiser, C. Thorpe, and D. Fass. 2006. Generating disulfides enzymatically: reaction products and electron acceptors of the endoplasmic reticulum thiol oxidase Ero1p. *Proceedings of the National Academy of Sciences of the United States of America*. 103:299-304.

Gutscher, M., M.C. Sobotta, G.H. Wabnitz, S. Ballikaya, A.J. Meyer, Y. Samstag, and T.P. Dick. 2009. Proximity-based protein thiol oxidation by H2O2-scavenging peroxidases. *The Journal of biological chemistry*. 284:31532-31540.

Hanson, G.T., R. Aggeler, D. Oglesbee, M. Cannon, R.A. Capaldi, R.Y. Tsien, and S.J. Remington. 2004. Investigating mitochondrial redox potential with redox-sensitive green fluorescent protein indicators. *The Journal of biological chemistry*. 279:13044-13053.

Hudson, D.A., S.A. Gannon, and C. Thorpe. 2014. Oxidative protein folding: From thiol-disulfide exchange reactions to the redox poise of the endoplasmic reticulum. *Free radical biology & medicine*.

Iuchi, Y., F. Okada, S. Tsunoda, N. Kibe, N. Shirasawa, M. Ikawa, M. Okabe, Y. Ikeda, and J. Fujii. 2009. Peroxiredoxin 4 knockout results in elevated spermatogenic cell death via oxidative stress. *The Biochemical journal*. 419:149-158.

Lohman, J.R., and S.J. Remington. 2008. Development of a family of redox-sensitive green fluorescent protein indicators for use in relatively oxidizing subcellular environments. *Biochemistry*. 47:8678-8688.

Malinouski, M., Y. Zhou, V.V. Belousov, D.L. Hatfield, and V.N. Gladyshev. 2011. Hydrogen peroxide probes directed to different cellular compartments. *PloS one*. 6:e14564.

Markvicheva, K.N., D.S. Bilan, N.M. Mishina, A.Y. Gorokhovatsky, L.M. Vinokurov, S. Lukyanov, and V.V. Belousov. 2011. A genetically encoded sensor for H2O2 with expanded dynamic range. *Bioorganic & medicinal chemistry*. 19:1079-1084.

Mehmeti, I., S. Lortz, and S. Lenzen. 2012. The H2O2-sensitive HyPer protein targeted to the endoplasmic reticulum as a mirror of the oxidizing thiol-disulfide milieu. *Free radical biology & medicine*. 53:1451-1458.

Pollard, M.G., K.J. Travers, and J.S. Weissman. 1998. Ero1p: a novel and ubiquitous protein with an essential role in oxidative protein folding in the endoplasmic reticulum. *Molecular cell*. 1:171-182.

Tavender, T.J., and N.J. Bulleid. 2010. Peroxiredoxin IV protects cells from oxidative stress by removing H2O2 produced during disulphide formation. *Journal of cell science*. 123:2672-2679.

Tavender, T.J., J.J. Springate, and N.J. Bulleid. 2010. Recycling of peroxiredoxin IV provides a novel pathway for disulphide formation in the endoplasmic reticulum. *The EMBO journal*. 29:4185-4197.

Tiedge, M., S. Lortz, J. Drinkgern, and S. Lenzen. 1997. Relation between antioxidant enzyme gene expression and antioxidative defense status of insulin-producing cells. *Diabetes*. 46:1733-1742.

Tiedge, M., S. Lortz, R. Munday, and S. Lenzen. 1998. Complementary action of antioxidant enzymes in the protection of bioengineered insulin-producing RINm5F cells against the toxicity of reactive oxygen species. *Diabetes*. 47:1578-1585.

Tien, A.C., A. Rajan, K.L. Schulze, H.D. Ryoo, M. Acar, H. Steller, and H.J. Bellen. 2008. Ero1L, a thiol oxidase, is required for Notch signaling through cysteine bridge formation of the Lin12-Notch repeats in Drosophila melanogaster. *The Journal of cell biology*. 182:1113-1125.

Tsai, B., and T.A. Rapoport. 2002. Unfolded cholera toxin is transferred to the ER membrane and released from protein disulfide isomerase upon oxidation by Ero1. *The Journal of cell biology*. 159:207-216.

Tsunoda, S., E. Avezov, A. Zyryanova, T. Konno, L. Mendes-Silva, E. Pinho Melo, H.P. Harding, and D. Ron. 2014. Intact protein folding in the glutathione-depleted endoplasmic reticulum implicates alternative protein thiol reductants. *eLife*. 3:e03421.

van Lith, M., S. Tiwari, J. Pediani, G. Milligan, and N.J. Bulleid. 2011. Real-time monitoring of redox changes in the mammalian endoplasmic reticulum. *Journal of cell science*. 124:2349-2356.

Zheng, M., F. Aslund, and G. Storz. 1998. Activation of the OxyR transcription factor by reversible disulfide bond formation. *Science*. 279:1718-1721.

Zito, E., K.T. Chin, J. Blais, H.P. Harding, and D. Ron. 2010a. ERO1-beta, a pancreas-specific disulfide oxidase, promotes insulin biogenesis and glucose homeostasis. *The Journal of cell biology*. 188:821-832.

Zito, E., H.G. Hansen, G.S. Yeo, J. Fujii, and D. Ron. 2012. Endoplasmic reticulum thiol oxidase deficiency leads to ascorbic acid depletion and noncanonical scurvy in mice. *Molecular cell*. 48:39-51.

Zito, E., E.P. Melo, Y. Yang, A. Wahlander, T.A. Neubert, and D. Ron. 2010b. Oxidative protein folding by an endoplasmic reticulum-localized peroxiredoxin. *Molecular cell*. 40:787-797.

## Figure Legends:

### Figure 1.

**PRDX4 supports near normal rate of ER thiol oxidation rates in the absence of ERO1.**

(A) Immunoblot of endogenous Ero1α, Ero1β and Prdx4 in lysates of MEFs with the indicated genotypes: wildtype (WT), *Ero1α; Ero1β* double-mutant (DKO), *Ero1α; Ero1β; Prdx4* triple mutant (TKO) and *Prdx4* single mutant (PKO). An-anti Actin blot, serves as loading control.

(B) Fluorescent photomicrographs of MEF cells transiently expressing ERroGFP2, immunostained for Calreticulin as an ER marker. The merge panels show an overlap of the GFP signal with Calreticulin and the karyophilic dye Hoechst 33258 (to reveal the nuclei).

(C-G) Traces of time-dependent changes in the fluorescence excitation ratio, reflecting the alterations in the oxidation state of roGFP2 expressed in the ER of cells with the indicated genotypes: WT, DKO, TKO and TKO expressing an active, $PRDX4^{WT}$, or inactive, $PRDX4^{C127S}$, enzyme. Cells were exposed to a brief (1 min) reductive pulse of dithiothreitol (DTT, 2 mM) followed by a washout. Each line traces the fluorescence profile of an individual cell.

(H) Bar diagram of the half-time to recovery of the oxidized form of ERroGFP2 following the reductive DTT pulse, calculated from fitting the data in C-G. Shown are means ±SEM ($n > 20$, $*p<0.05$, $**p<0.01$)

## Figure 2.

**ERHyPer responds to exogenous $H_2O_2$ in a chemically imposed reducing environment**

(A) Plot of rate of in vitro oxidation of HyPer (1 μM) as function of $H_2O_2$ or $PDI^{OX}$ concentration, calculated from the linear phase of the initial oxidation reaction traced ratiometrically (Fig. S2).

(B) Schema representing response modes of ERroGFP2 and ERHyper. Both probes undergo oxidation by PDI. But unlike roGFP2, reduced HyPer also undergoes rapid oxidation by $H_2O_2$. Thus HyPer's responsiveness to $H_2O_2$ can be unmasked in settings with low concentration of oxidized PDI.

(C) Traces of time dependent changes to the redox sensitive excitation ratio of HyPer exposed to various concentrations of $H_2O_2$ in vitro, in the continued presence of DTT.

(D) Fluorescent photomicrographs of MEFs transiently transfected with ERHyPer encoding vector, immunostained for calreticulin, as an ER marker.

(E) Trace of time-dependent changes to the oxidation state of ERHyPer (upper plot) or ERroGFP2 (lower plot) expressed in MEF cells challenged repeatedly with $H_2O_2$ (arrows) in the continuous presence of DTT. The general oxidant, Diamide, was added in excess, to reveal the responsiveness of both probes at the end of the experiment.

(F) Trace of time dependent changes to the redox state of ERHyPer expressed in MEF cells, first briefly exposed to DTT, followed by wash out; then exposure to DTT, followed by introduction of $H_2O_2$ to the reducing medium.

## Figure 3.

**Sluggish transit of $H_2O_2$ into the ER lumen**

(A) Plot showing the dependence of the redox state of cytosolically-localised Hyper (cytoHyPer) expressed RINm5F cells (measured by excitation ratio) on concentration of $H_2O_2$, introduced to the culture medium in the continued presence or absence of DTT (2mM).

(B) Plot of the relationship between HyPer oxidation state (linearly normalized, by setting the maximal observed value to 1 and the minimal observed value to zero) in the different compartments and concentration of $H_2O_2$ in the media in RINm5F cells exposed continuously to DTT (as in "A").

(C) Bar diagram of the mean $H_2O_2$ concentration in the culture media required to effect 50% of maximal oxidation of cytosolic, mitochondrial, or ER localized HyPer (the midpoint in the traces shown in "B" above)(mean ± SEM, n=4, **P < 0.01).

(D) Titration of $H_2O_2$ as described in (C), performed in presence of DTT in RINm5F or MEF cells. Note the enhanced sensitivity of RINm5F cells compared to the MEFs

## Figure 4.

**Purging the ER of its $H_2O_2$ content selectively retards PRDX4 mediated ER oxidation.**

(A) Bar diagram showing specific activities of catalase in extracts of untransfected $MEF^{DKO}$ cells and cells expressing catalase variants targeted to the indicated compartments.

(B-D) Plot of the relationship between $H_2O_2$ concentration in the media and the excitation ratio of cytoHyper, mitoHyPer or ERHyPer, expressed alone or alongside catalase in $MEF^{DKO}$ cells (with insets of fixed anti-catalase immunostained cells showing the localization of the protein). The titration measuring the ER localized probe was performed in presence of DTT (2mM). The plots are presented along their corresponding ratiometric photomicrographs (B-D lower panels). The catalase-expressing cells are marked by the co-expression of mCherry (encoded on the same plasmid, denoted by white arrows). Note, the ratio indicating a more reduced state (color coded in blue-green) at the intermediate $H_2O_2$ concentration in catalase positive cells compared to mostly oxidized state (color codded yellow-red) in catalase negative cells, as the later are desensitized to $H_2O_2$ by catalase overexpression.

(E) Traces of oxidation recovery of ERroGFP2 following a DTT pulse (2 mM, 1 min) in $MEF^{DKO}$ cells with catalase expressed in the indicated compartments.

(F) Bar diagram of the half-time to recovery of the oxidized form of ERroGFP2 following the reductive DTT pulse, calculated from fitting the data in (E). Shown are means $t_{1/2}$ ±SEM ($n > 10$, $*p<0.01$)

(G) Traces of oxidation recovery of ERroGFP2 following a DTT (2mM, 1 min) pulse in parental TKO cells [Cat(-)] and TKO cells expressing catalase in their ER [ER Cat], identified by the presence of the co-expressed mCherry marker, as in (E-G)]. Inset shows a bar diagram of the corresponding ERroGFP2 re-oxidation half-time values. Shown are mean ±SEM ($n > 10$)

# Supplemental Figure Legends:

## Figure S1.

**No evidence for a contribution of PRDX4 to the rate of disulfide bond formation in ERO1-expressing cells.**

Traces of time-dependent changes in the fluorescence excitation ratio, reflecting the alterations in the oxidation state of roGFP2 expressed in the ER of PRDX4 knockout mouse lung fibroblasts (PKO) or their isogenic control (WT). Cells were exposed to a brief (1 min) reductive pulse (dithiothreitol, DTT, 2 mM) followed by a washout. Each line traces the ratio in an individual cell (values shown denote mean recovery $t_{1/2}$ ±SEM, n>10).

## Figure S2.

**Kinetics of HyPer oxidation by $H_2O_2$ or PDI in vitro and in vivo**

Trace of time-dependent changes in the fluorescence excitation ratio of reduced HyPer (1mM) exposed to the indicated concentrations of $H_2O_2$ (A) or oxidized PDI (B) in vitro; and of roGFP2 (A) or HyPer (B) expressed in the ER of cells lacking ERO1 and PRDX4 ($MEF^{TKO}$); a brief (1 min) reductive pulse (dithiothreitol, DTT, 2 mM) was followed by a washout, during which $H_2O_2$ (100 mM) was added. Shown are traces of the ratio in individual cells.

Fig. 1

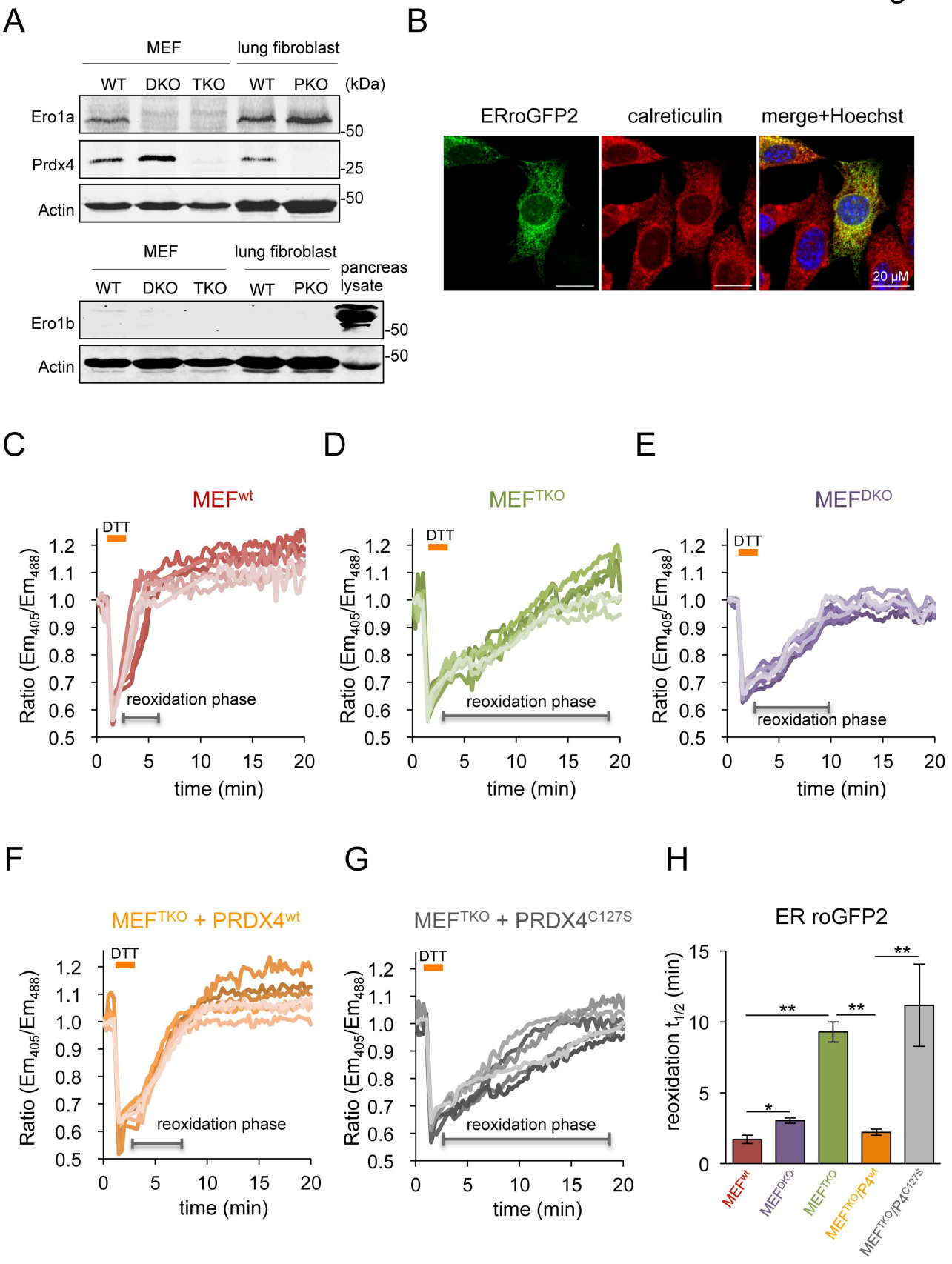
A
MEF
lung fibroblast
WT
DKO
TKO
WT
PKO
(kDa)
Ero1a
-50
Prdx4
-25
Actin
-50
MEF
lung fibroblast
pancreas lysate
WT
DKO
TKO
WT
PKO
Ero1b
-50
Actin
-50
B
ERroGFP2
calreticulin
merge+Hoechst
20 µM
C
MEFwt
DTT
Ratio (Em405/Em488)
reoxidation phase
time (min)
D
MEFTKO
DTT
Ratio (Em405/Em488)
reoxidation phase
time (min)
E
MEFDKO
DTT
Ratio (Em405/Em488)
reoxidation phase
time (min)
F
MEFTKO + PRDX4wt
DTT
Ratio (Em405/Em488)
reoxidation phase
time (min)
G
MEFTKO + PRDX4C127S
DTT
Ratio (Em405/Em488)
reoxidation phase
time (min)
H
ER roGFP2
reoxidation t1/2 (min)
MEFwt
MEFDKO
MEFTKO
MEFTKO/P4wt
MEFTKO/P4C127S

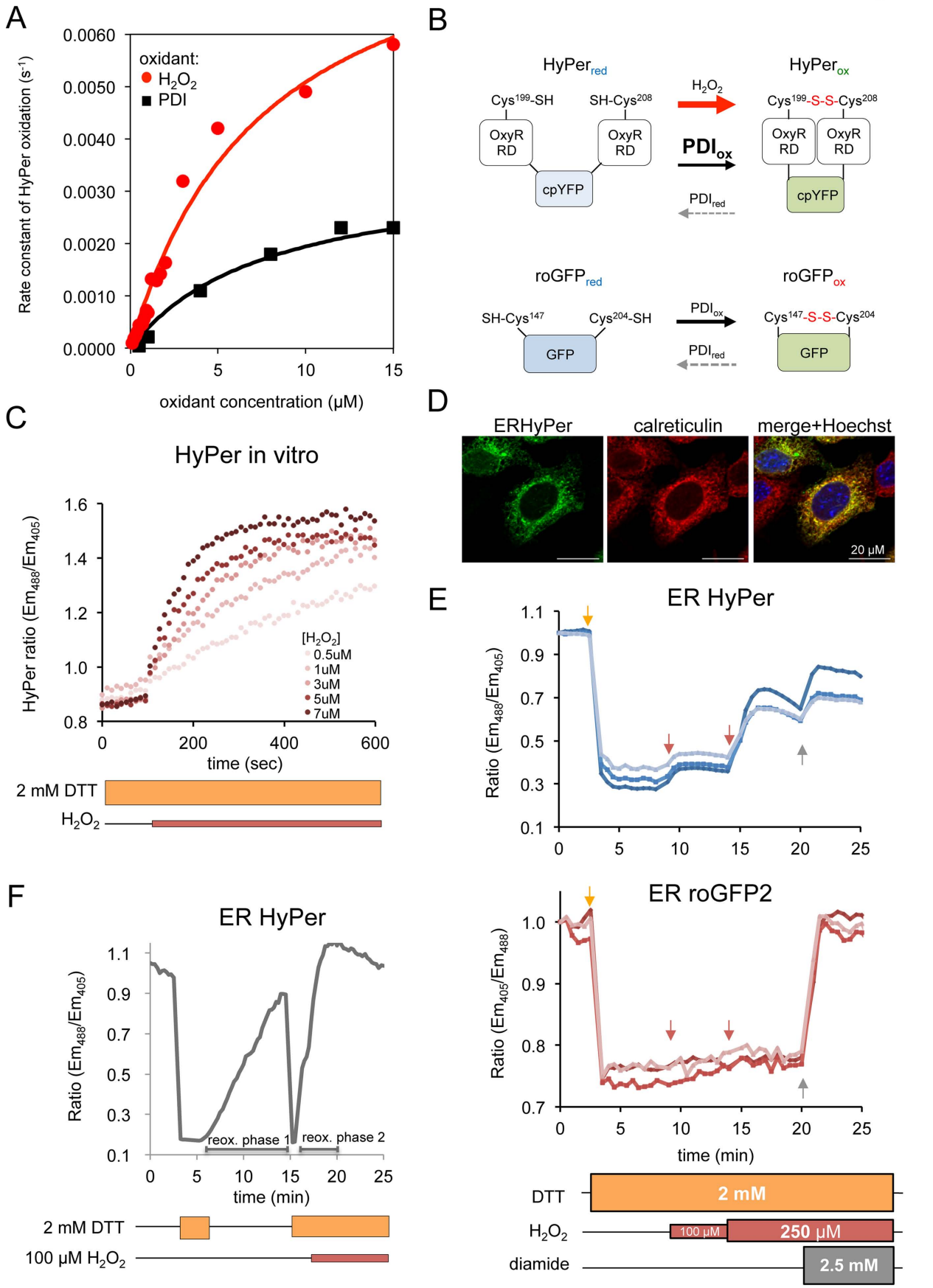
A
Rate constant of HyPer oxidation (s-1)
oxidant:
H2O2
PDI
oxidant concentration (μM)
B
HyPerred
HyPerox
Cys199-SH
SH-Cys208
Cys199-S-S-Cys208
OxyR RD
cpYFP
H2O2
PDIox
PDIred
roGFPred
roGFPox
SH-Cys147
Cys204-SH
Cys147-S-S-Cys204
GFP
C
HyPer in vitro
HyPer ratio (Em488/Em405)
[H2O2]
0.5uM
1uM
3uM
5uM
7uM
time (sec)
2 mM DTT
H2O2
D
ERHyPer
calreticulin
merge+Hoechst
20 μM
E
ER HyPer
Ratio (Em488/Em405)
F
ER HyPer
Ratio (Em488/Em405)
reox. phase 1
reox. phase 2
time (min)
2 mM DTT
100 μM H2O2
ER roGFP2
Ratio (Em405/Em488)
time (min)
DTT
2 mM
H2O2
100 μM
250 μM
diamide
2.5 mM

Fig. 3

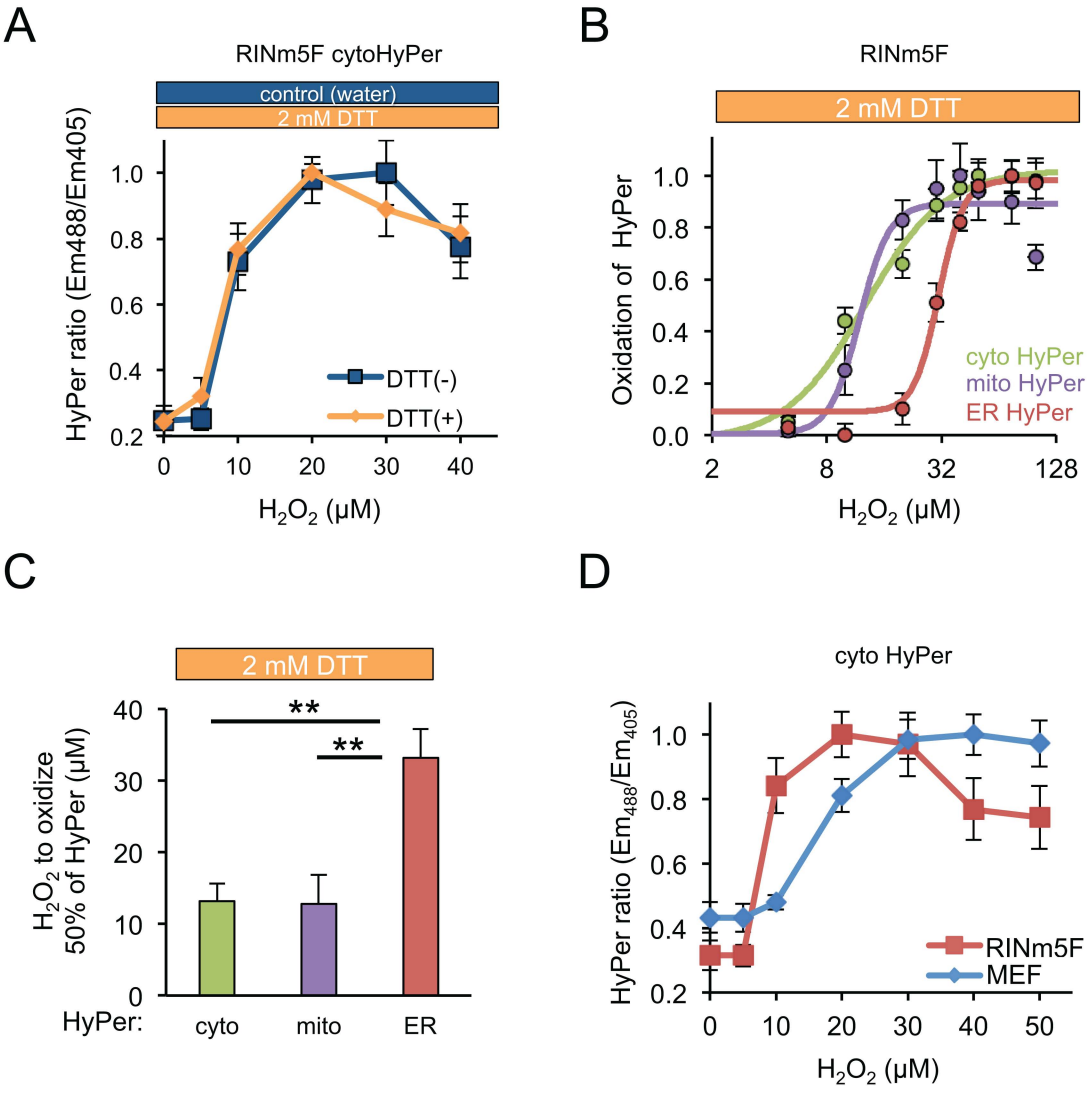
A
RINm5F cytoHyPer
control (water)
2 mM DTT
HyPer ratio (Em488/Em405)
1.0
0.8
0.6
0.4
0.2
0
10
20
30
40
DTT(-)
DTT(+)
H2O2 (μM)
B
RINm5F
2 mM DTT
Oxidation of HyPer
1.0
0.8
0.6
0.4
0.2
0.0
2
8
32
128
cyto HyPer
mito HyPer
ER HyPer
H2O2 (μM)
C
2 mM DTT
H2O2 to oxidize 50% of HyPer (μM)
40
30
20
10
0
**
**
HyPer:
cyto
mito
ER
D
cyto HyPer
HyPer ratio (Em488/Em405)
1.0
0.8
0.6
0.4
0.2
0
10
20
30
40
50
RINm5F
MEF
H2O2 (μM)

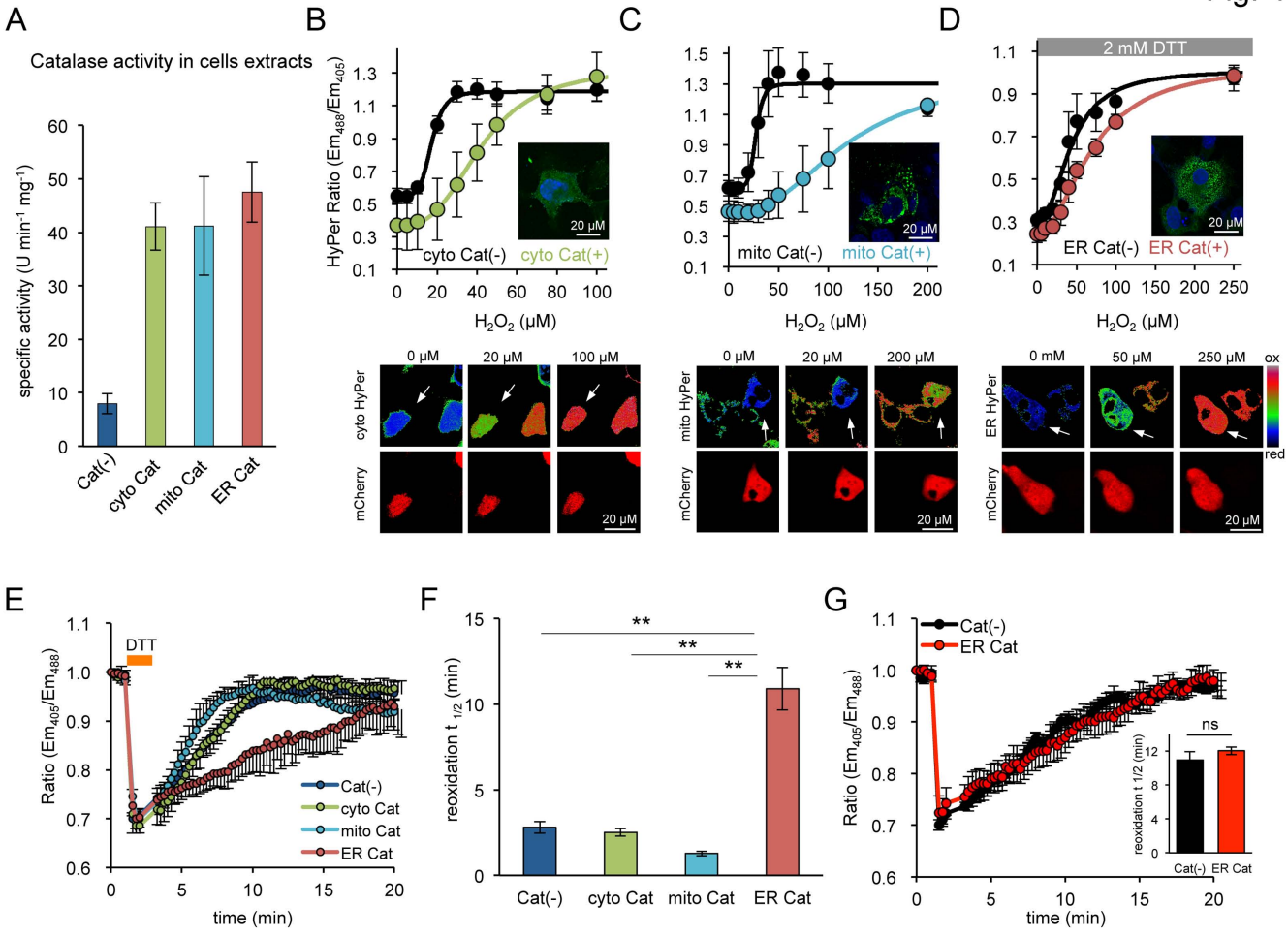
A
Catalase activity in cells extracts
specific activity (U min-1 mg-1)
Cat(-)
cyto Cat
mito Cat
ER Cat
B
HyPer Ratio (Em488/Em405)
cyto Cat(-)
cyto Cat(+)
H2O2 (μM)
20 μM
0 μM
20 μM
100 μM
cyto HyPer
mCherry
C
mito Cat(-)
mito Cat(+)
H2O2 (μM)
0 μM
20 μM
200 μM
mito HyPer
mCherry
D
2 mM DTT
ER Cat(-)
ER Cat(+)
H2O2 (μM)
0 mM
50 μM
250 μM
ox
red
ER HyPer
mCherry
E
DTT
Ratio (Em405/Em488)
Cat(-)
cyto Cat
mito Cat
ER Cat
time (min)
F
reoxidation t 1/2 (min)
**
**
**
Cat(-)
cyto Cat
mito Cat
ER Cat
G
Cat(-)
ER Cat
Ratio (Em405/Em488)
ns
reoxidation t 1/2 (min)
Cat(-)
ER Cat
time (min)

Fig. S1

A

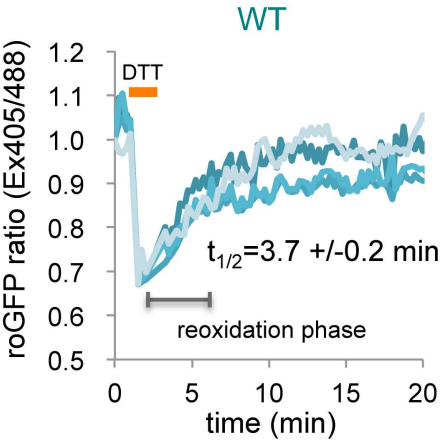
WT
DTT
roGFP ratio (Ex405/488)
1.2
1.1
1.0
0.9
0.8
0.7
0.6
0.5
$t_{1/2}$=3.7 +/-0.2 min
reoxidation phase
0
5
10
15
20
time (min)

B

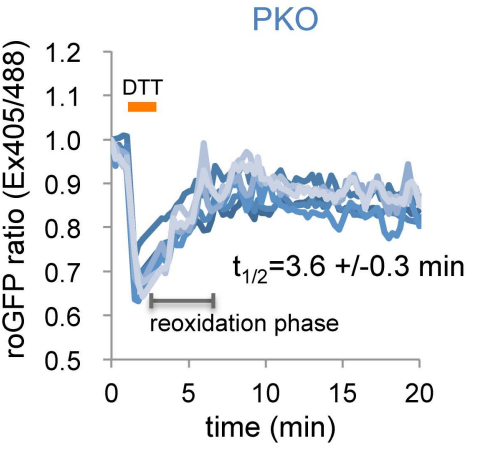
PKO
DTT
roGFP ratio (Ex405/488)
1.2
1.1
1.0
0.9
0.8
0.7
0.6
0.5
$t_{1/2}$=3.6 +/-0.3 min
reoxidation phase
0
5
10
15
20
time (min)

Fig. S2

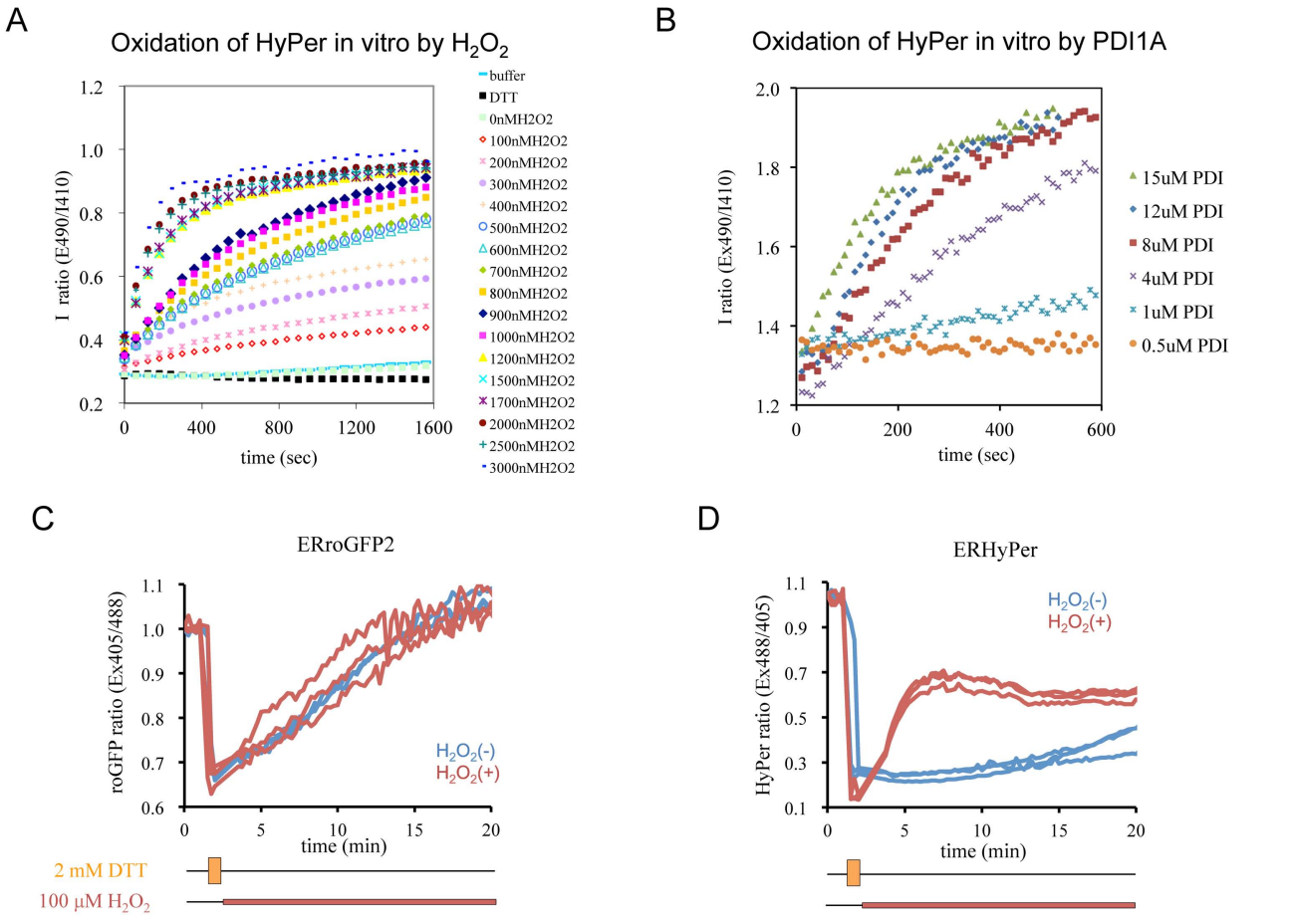
A
Oxidation of HyPer in vitro by $H_2O_2$
I ratio (E490/1410)
time (sec)
buffer
DTT
0nMH2O2
100nMH2O2
200nMH2O2
300nMH2O2
400nMH2O2
500nMH2O2
600nMH2O2
700nMH2O2
800nMH2O2
900nMH2O2
1000nMH2O2
1200nMH2O2
1500nMH2O2
1700nMH2O2
2000nMH2O2
2500nMH2O2
3000nMH2O2
B
Oxidation of HyPer in vitro by PDI1A
I ratio (Ex490/1410)
time (sec)
15uM PDI
12uM PDI
8uM PDI
4uM PDI
1uM PDI
0.5uM PDI
C
ERroGFP2
roGFP ratio (Ex405/488)
time (min)
$H_2O_2$(-)
$H_2O_2$(+)
2 mM DTT
100 μM $H_2O_2$
D
ERHyPer
HyPer ratio (Ex488/405)
time (min)
$H_2O_2$(-)
$H_2O_2$(+)

Table S1.

| ID | Plasmid name | Description | Reference | First appearance | Label in figure |
|---|---|---|---|---|---|
| 1052 | FLAGM1_roGFP2_pCDNA3.1 | Mammalian expression, ER-localized roGFP2 | PMID: 25073928 | Figure 1 | ERroGFP2 |
| 1187 | mPRDX4_37-274_WT_pFLAG_CMV1 | Mammalian expression of mouse PRDX4 | this study | Figure 1 | PRDX4 wt |
| 1188 | mPRDX4_37-274_C127S_pFLAG_CMV1 | Mammalian expression of mouse PRDX4 inactive mutant | this study | Figure 1 | PRDX4 C127S |
| 233 | hPDI(18-508)pTrcHis-A | Bacterial expression of human PDI1A | PMID: 21145486 | Figure 2 | PDI |
| 778 | pHyper_pQE30 | Bacterial expression HyPer | PMID: 16554833 | Figure 2 | HyPer |
| 855 | pFLAG_ERHyPerA233V_CMV1 | Mammalian expression, cytosolic HyPer2 | this study, based on PMID: 20692175 | Figure 2 | ERHyPer |
| 1361 | Cyto HyPer_A233V | Mammalian expression, mitochondrial HyPer2 | this study, based on PMID: 20692175 | Figure 3 | cytoHyPer |
| 1362 | mito HyPer_A233V | Mammalian expression, ER targeted HyPer2 | this study, based on PMID: 20692175 | Figure 3 | mitoHyPer |
| 1402 | hCatase_cyto_pCEFL_mCherry | Mammalian expression of cytosolic human catalase and mCherry from separate promoters | this study | Figure 4 | cytoCat |
| 1404 | hCatase_mito_pCEFL_mCherry | Mammalian expression of mitochondrial human catalase and mCherry from separate promoters | this study | Figure 4 | mitoCat |
| 1438 | hCatase_ER_pCEFL_mCherry | Mammalian expression of ER human catalase and mCherry from separate promoters (ER active variant) | this study, based on PMID: 25499853 | Figure 4 | ERCat |